# Vibrational and electronic properties of neutral and negatively charged $C_{20}$ clusters

Giulia Galli and François Gygi

*Institut Romand de Recherche Numérique en Physique des Matériaux, CH-1015 Lausanne, Switzerland*

J.-Christophe Golaz*

*Institut de Physique Appliquée, Ecole Polytechnique Fédérale de Lausanne, CH-1015 Lausanne, Switzerland*
(Received 3 September 1997)

We computed vibrational and electronic properties of the cage, bowl, and ring isomers of neutral and negatively charged $C_{20}$, within density-functional theory, using fully optimized local-density and gradient-corrected geometries. Vibrational and electronic spectra exhibit distinctive features, which could be used to identify a given isomer and its charge state in molecular beams or thin films. Notable changes are observed in both the Raman and infrared spectra when going from the neutral to the charged isomers. We also calculated vibrational entropies from harmonic frequencies. Our results indicate that, above a critical temperature, the ring isomer is always stabilized by entropic effects, irrespective of the theoretical model used to compute the internal energy. In particular, gradient-corrected functionals predict both the neutral and charged ring to be the most stable isomer at all temperatures. Molecular-dynamics simulations were performed to study the geometry of the ring at high temperature. Furthermore, we rationalized photoelectron spectra of $C_{2n}$ clusters, $n = 9–12$, in terms of differences in the electronic structure for even and odd $n$. [S0163-1829(98)07403-7]

## I. INTRODUCTION

The geometric structure of small carbon clusters is of basic interest to the understanding of fullerene formation,[1,2] as well as of the microscopic structure of fullerene assembled thin films.[3–5] Among the carbon clusters with less than 60 atoms, $C_{20}$ is the smallest molecule that could form a fullerene cage and has been the subject of many investigations in recent years, by both chemists and physicists.[6–18] However, the relative stability of the different $C_{20}$ isomers is still the subject of controversy. In particular, there is an apparent disagreement between experiments[6–9] indicating that the dominant species in graphite laser vaporization sources is a ring structure, and most first-principles calculations, finding either the cage or the bowl as most stable isomers at zero temperature. We note that most experiments are carried out for negatively charged species, whereas *ab initio* calculations have so far been performed for neutral molecules. Furthermore, ion chromatography,[6] ion drift experiments,[7] and ultraviolet photoemission spectroscopy patterns[8] favor a monocyclic ring geometry, whereas photoelectron spectroscopy data[9] have been interpreted in terms of bicyclic rings.

In this paper we present a first-principles theoretical study of the vibrational and electronic properties of the cage, bowl, and ring isomers of both neutral and negatively charged $C_{20}$. We have fully optimized the geometries of all isomers at the local-density and gradient-corrected level.[19] Our results allow us to identify distinctive features of each isomer in both electronic and vibrational spectra, and to evaluate free energies within the harmonic approximation. This permits the study of the relative stability of the three isomers as a function of temperature, and the investigations of the changes occurring in their vibrational and electronic properties when going from neutral to charged species. Furthermore, we present a comparative analysis of the electronic properties of $C_{18}$ and $C_{20}$ neutral rings, which allows one to interpret recent experiments[9] without invoking the presence of bicyclic ring structures.

## II. GROUND-STATE GEOMETRIES AND ELECTRONIC SPECTRA

We carried out density-functional calculations using norm-conserving pseudopotentials and plane-wave basis sets,[23] with a kinetic-energy cutoff of 40 Ry and a $(30 \text{ a.u.})^3$ unit cell. We used both the local-density approximation (LDA) and the generalized gradient approximation recently proposed by Perdew, Burke, and Ernzerhof (PBE) (Ref. 19) and successfully used to study molecular systems.[20,21] In the case of neutral clusters, we checked the effect of periodic boundary conditions and of finite cell size by computing total energies in a larger cell $[(40 \text{ a.u.})^3]$, which led to energy changes smaller than 1 meV. In the case of charged clusters, the energy differences between different isomers are correct up to $O(L^{-3})$, where $L$ is the edge of the cubic cell used in our calculations; the linear terms in $L$ cancel out, being dependent only on the shape of the cell.[22]

The optimized geometries of neutral $C_{20}$ at $T = 0$ are shown in Fig. 1 and the relative total energies are displayed in Table I, together with results published in the literature. When using LDA, similar to former calculations[10–12,17] we found that the cage is the most stable structure at $T = 0$, followed by the bowl and the ring, in order of increasing energy. We checked basis set convergence by increasing the kinetic-energy cutoff to 60 Ry, which changed the relative energies of the cage, bowl, and ring by 0.1–0.2 eV, but did not affect the energy ordering. When using PBE, we found that the most stable structure is the ring, followed by the bowl and the cage, in agreement with other gradient-corrected calculations using LDA optimized geometries.[16,17]

The symmetry of the fully optimized structures (see Fig. 1) of the neutral cage, bowl, and ring are $D_{3d}$, $C_{5v}$, and
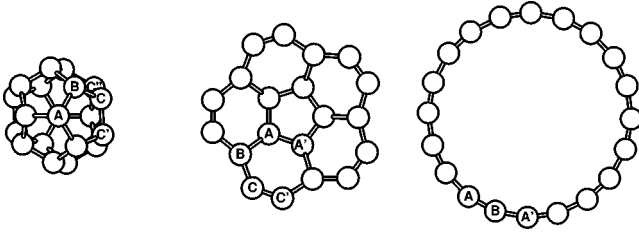
FIG. 1. Geometries of the three neutral $C_{20}$ isomers: the cage ($D_{3d}$), the bowl ($C_{5v}$), and the ring ($D_{10h}$). The four characteristic bond lengths ($d$) of the cage are $d_{CC''}=1.409$, $d_{AB}=1.443$, $d_{BC}=1.450$, and $d_{CC'}=1.512$ Å; those of the bowl are $d_{CC'}=1.249$, $d_{BC}=1.410$, $d_{AA'}=1.423$, and $d_{AB}=1.434$ Å; those of the ring are $d_{AB}=1.244$ and $d_{BA'}=1.334$ Å. These results have been obtained with 40 Ry cutoff. Atoms labeled with the same letter are equivalent.

$D_{10h}$, respectively, for both LDA and PBE calculations. Although the relative stability of the three isomers is different within LDA and PBE, fully optimized geometries are very similar. In our calculations the cage and the bowl have four characteristic bond lengths whereas the ring exhibits alternating short and long bonds (we call this a dimerized ring geometry). Table II shows optimized geometries obtained in

TABLE I. Relative energies (eV) of the three neutral $C_{20}$ isomers as calculated with different theoretical models. We show results obtained with the LDA and using gradient corrected functionals. These functionals use Becke exchange with one ($B$) or three ($B3$) fitting parameters and the correlation formulas proposed by Lee, Yang, and Parr (LYP), Perdew and Wang (PW91) and PBE. Results of CCSD(T) (coupled-cluster single and double excitations with triple excitations added perturbatively) and diffusion quantum Monte Carlo (QMC) calculations are shown for comparison. Geometries are optimized at the LDA (/LDA), Hartree-Fock (/HF) or PBE (/PBE) level. For our LDA calculations, both results obtained with a plane-wave cutoff ($E_{cut}$) of 40 and 60 Ry are shown (see text). For each theoretical model, we set to zero the total energy of the most stable structure.

| Theoretical model | Cage | Bowl | Ring |
|---|---|---|---|
| LDA/LDA (this work; $E_{cut}=40$ Ry) | 0.00 | 0.75 | 2.76 |
| LDA/LDA (this work; $E_{cut}=60$ Ry) | 0.00 | 0.64 | 2.51 |
| LDA/LDA (Ref. 10) | 0.00 | 0.75 | 2.65 |
| LDA/LDA (Ref. 11) | 0.00 | 0.80 | 2.30 |
| LDA/LDA (Ref. 12) | 0.00 | 1.46 | 3.85 |
| LDA/HF (Ref. 14) | 0.00 | 1.12 | 4.10 |
| $P$BE/$P$BE (this work; $E_{cut}=40$ Ry) | 1.00 | 0.17 | 0.00 |
| $B$-LYP/HF (Ref. 13) | 3.43 | 1.07 | 0.00 |
| $B$-LYP/LDA (Ref. 12) | 3.32 | 1.50 | 0.00 |
| $B3$-LYP/HF (Ref. 14) | 2.33 | 0.40 | 0.00 |
| $B3$-LYP/HF (Ref. 16) | 1.33 | 0.00 | 0.60 |
| $B3$-LYP/LDA (Ref. 16) | 1.42 | 0.52 | 0.00 |
| $B$-PW91/HF (Ref. 14) | 0.78 | 0.00 | 0.47 |
| $B3$-PW91/HF (Ref. 14) | 0.72 | 0.00 | 0.82 |
| CCSD($T$)/LDA (Ref. 11) | 0.00 | 0.00 | 1.7 |
| CCSD($T$)/HF (Ref. 11) | 0.60 | 0.00 | 2.8 |
| QMC/HF (Ref. 14) | 2.2 | 0.00 | 1.1 |

various calculations. In general, geometries optimized at the Hartree-Fock (HF) and LDA levels are considerably different. In particular, for the ring, the difference in length between short and long bonds (dimerization) obtained with HF calculations is much larger ($\simeq 0.2$ Å) than that yielded by LDA calculations ($\simeq 0.07$ Å). All published LDA calculations give similar geometries for both the bowl and the ring, whereas the results for the cage differ appreciably. We obtain a $D_{3d}$ symmetry, while most other authors find structures of lower symmetry ($C_2$ or $C_i$). Such low symmetry structures may result from an incomplete optimization of the ionic coordinates of the fullerene cage. In our calculations full convergence was attained by requiring ionic forces to be smaller than $10^{-5}$ a.u., a more stringent criterion than that used, e.g., in Ref. 12 ($10^{-3}$ a.u.). We also computed the LDA total energy of the fullerene cage using the geometry proposed in Ref. 13 ($C_2$ symmetry, optimized at the HF level) and found it to be 1.30 eV higher than the energy of our optimized cage geometry.

Similarly to neutral clusters, when using LDA we found that the cage is the most stable isomer of $C_{20}^-$, whereas the ring is the ground-state structure within PBE. Our results are summarized in Table III. The optimized geometries of the negatively charged clusters (see Table IV) show important differences with respect to those of the neutral counterparts. The cage symmetry is lowered to $C_{2h}$ and bond distances vary between 1.40 and 1.51 Å. The bowl symmetry is lowered to $C_2$ when using PBE, whereas it is preserved to $C_{5v}$ within LDA. We note that the symmetry breaking is rather small. In both cases the shortest interatomic distances of the cluster increase and the longest distances decrease with respect to the neutral species. In the ring, the symmetry is preserved and the dimerization is slightly reduced, the LDA and PBE results being very similar.

Figure 2 shows the density of electronic states (DOS) of the three $C_{20}$ isomers both in the neutral (solid line) and charged (dotted line) states. The bandwidths are sensibly different for the three geometries, the cage's being the widest (20.75 eV for neutral $C_{20}$), followed by the bowl's (17.29 eV) and the ring's (15.74 eV). A distinctive feature of the ring spectrum is the presence of a large gap ($\simeq 3$ eV) separating $\sigma$ from $\pi$ states, which does not have any analogue in the bowl and cage spectra. This feature is a consequence of the ring having a quasi-one-dimensional geometry. We also notice the marked difference between the neutral cage and bowl spectra near the highest occupied molecular orbital, where the bowl DOS exhibits a sharp edge, whereas the cage DOS vanishes more gently.

The DOS of the charged ring and bowl are very similar to those of their neutral counterparts, showing just one extra state close to the highest occupied state. The DOS of the charged cage is instead modified with respect to that of the neutral isomer over an energy range of about 10 eV close to the highest occupied orbital, although also in this case the differences are small.

## III. VIBRATIONAL SPECTRA AND FREE ENERGY

We determined the harmonic vibrational frequencies ($\omega_i$) of each isomer (Tables V and VI) by diagonalizing the (60 $\times$ 60) matrix,

TABLE II. Symmetry and bond lengths of the three isomers of neutral $C_{20}$ as optimized in our calculations (this work) at the LDA and gradient-corrected (PBE) level, compared to those published in the literature both at the LDA and HF level.

| Isomer | Geometry optimization | Symmetry | Bond lengths (Å) |
|---|---|---|---|
| Cage | LDA (this work) | $D_{3d}$ | 1.409, 1.443, 1.450, 1.51 |
| | PBE (this work) | $D_{3d}$ | 1.407, 1.443, 1.450, 1.51 |
| | LDA (Ref. 10) | | 1.42-1.49 |
| | LDA (Ref. 12) | $C_i$ | 1.395-1.517 |
| | LDA-BLYP (Ref. 12) | $C_i$ | 1.405-1.542 |
| | HF (Ref. 12) | $C_2$ | 1.368-1.504 |
| | HF (Ref. 13) | $C_2$ | 1.367-1.504 |
| | HF (Ref. 15) | $D_{5d}$ | 1.416, 1.425, 1.474 |
| Bowl | LDA (this work) | $C_{5v}$ | 1.249, 1.410, 1.423, 1.434 |
| | PBE (this work) | $C_{5v}$ | 1.246, 1.414, 1.425, 1.435 |
| | LDA (Ref. 10) | | 1.25, 1.40-1.45 |
| | LDA (Ref. 12) | $C_{5v}$ | 1.256, 1.404, 1.413, 1.415 |
| | LDA-BLYP (Ref. 12) | $C_{5v}$ | 1.258, 1.412, 1.418, 1.430 |
| | HF (Ref. 12) | $C_{5v}$ | 1.218, 1.397, 1.424, 1.429 |
| | HF (Ref. 13) | $C_{5v}$ | 1.218, 1.397, 1.424, 1.429 |
| Ring | LDA (this work) | $D_{10h}$ | 1.244, 1.334 |
| | PBE (this work) | $D_{10h}$ | 1.241, 1.336 |
| | LDA (Ref. 10) | $C_{10h}$ | 1.25, 1.33 |
| | LDA (Ref. 12) | $C_{10h}$ | 1.245, 1.329 |
| | LDA-BLYP (Ref. 12) | $C_{10h}$ | 1.243, 1.333 |
| | HF (Ref. 12) | $C_{10h}$ | 1.196, 1.381 |
| | HF (Ref. 13) | $C_{10h}$ | 1.196, 1.381 |
| | HF (Ref. 15) | $D_{10h}$ | 1.193, 1.378 |

$$A_{ij} = \frac{1}{m_C} \frac{\partial^2 E_0}{\partial x_i \partial x_j}. \qquad (1)$$

Here $E_0$ denotes the total energy of the system at zero temperature, $x_i$ is one of the 60 displacements from equilibrium along the $x$, $y$, and $z$ directions of each atom, and $m_C$ is the mass of a C atom. The eigenvalues ($\lambda_i$) of $A$ are related to the eigenfrequencies $\omega_i$ by $\lambda_i = \omega_i^2$. In Eq. (1), $\partial^2 E_0/\partial x_i \partial x_j$ was calculated as $-(\partial F_i/\partial x_j)$, where $F_i$ denotes the force acting on $x_i$. The derivatives were evaluated by imposing small symmetric displacements (0.1 a.u.) from the equilibrium and then computing $F_i$ in the displaced configurations. The matrix elements of $A$ were obtained using a symmetric two-point finite difference formula, which eliminates the influence of any residual force at the reference equilibrium position.

TABLE III. Relative energies (eV) of the three isomers of negatively charged $C_{20}$ isomers as calculated with different theoretical models. We show results obtained with the LDA and using the gradient-corrected functional proposed by PBE. For each theoretical model, we set to zero the total energy of the most stable structure. Our results have been obtained using a plane-wave cutoff of 40 Ry.

| Theoretical model | Cage | Bowl | Ring |
|---|---|---|---|
| LDA | 0.00 | 0.49 | 1.83 |
| PBE | 1.89 | 1.14 | 0.00 |

Figures 3–7 show infrared (IR) and Raman ($R$) active frequencies of the $C_{20}$ isomers, and Tables IV and V display the full spectra of the neutral and charged isomers, respectively. We note that the symmetry groups of the cage and the ring contain the inversion operation and thus it is possible to discriminate between IR and $R$ active modes; on the contrary, the symmetry group of the bowl does not include the inversion and, therefore, no distinction can be drawn between IR and R active modes. There are profound differences between the vibrational properties of the three isomers of $C_{20}$ and important modifications of the spectra occur when charging the clusters.

We first discuss the spectra of the neutral molecules. The cage (Figs. 3–4) has 23 IR and 24 $R$ active modes, all of them below 1500 cm$^{-1}$. The IR spectrum lies between 500 and 1300 cm$^{-1}$ and the Raman frequencies are in the interval 500–1400 cm$^{-1}$, with a single line at a lower frequency ($\simeq 150$ cm$^{-1}$). The bowl (Fig. 5) has 50 IR and $R$ active modes in the range 150–1900 cm$^{-1}$, with a gap between 1500 and 1800 cm$^{-1}$. The ring has only four IR active modes (Fig. 6) — three in the range 400–500 cm$^{-1}$ and one at high frequency (1944 cm$^{-1}$) — and eight $R$ active modes (Fig. 7), one at very low (45 cm$^{-1}$) and two at very high (above 2000 cm$^{-1}$) frequencies. The spectrum computed for the ring structure agrees well with published LDA results.[12] We note that there are non-negligible differences between results obtained at the LDA and HF level,[12] especially in the high-frequency part of the spectrum. Our results

TABLE IV. Symmetry and bond lengths of the three isomers of negatively charged $C_{20}$ as optimized in our calculations at the LDA and gradient-corrected (PBE) level. The cage isomer has one very low vibrational frequency and the structural optimization of this structure is less accurate than that of the charged bowl and ring.

| Isomer | Geometry optimization | Symmetry | Bond lengths (Å) |
|--------|-----------------------|----------|------------------|
| Cage | LDA | $C_{2h}$ | 1.40, 1.41, 1.42-1.52 |
|      | PBE | $C_{2h}$ | 1.40, 1.41, 1.42-1.52 |
| Bowl | LDA | $C_{5v}$ | 1.270, 1.419, 1.426, 1.428 |
|      | PBE | $C_2$   | 1.251, 1.273, 1.413, 1.419, 1.428, 1.431 |
| Ring | LDA | $D_{10h}$ | 1.257, 1.324 |
|      | PBE | $D_{10h}$ | 1.255, 1.326 |

for the spectrum of the bowl agree reasonably well with those obtained using the B3LYP energy functional,[16] although in the high-frequency region we find modes that are not as stiff. On the contrary, there are sensible differences with the B3LYP results[16] for the cage, which were obtained for HF optimized $C_{2h}$ and $C_i$ geometries, especially in the low-frequency part of the spectrum.

When charging the cage, its IR frequencies are not sensibly modified (Fig. 3), whereas its $R$ spectrum shows notable changes (Fig. 4). In particular, an active mode appears at low frequency (28 cm$^{-1}$) and the gap between 150 and 500 cm$^{-1}$ is partially filled. The low-frequency mode corresponds to a higher-frequency inactive mode in the neutral cluster. In the bowl, we observe a change in the uppermost

part of the spectrum (Fig. 5), where the modes are shifted downward. Similarly the high frequency IR and $R$ modes of the ring are shifted downwards (Figs. 6 and 7).

We have used the computed total energy at zero temperature ($E_0$) and the harmonic frequencies to evaluate the free energy ($\mathcal{F}$) of the different $C_{20}$ isomers as a function of temperature ($T$), from the formula[24]

$$\mathcal{F}=E_0-\frac{1}{2}\sum_i \hbar\omega_i+k_BT\sum_i \ln\left(\exp\frac{\hbar\omega_i}{k_BT}-1\right). \quad (2)$$

The results are shown in Fig. 8 for LDA and PBE functionals. Within LDA, for $T\leq1100$ (700) K, we obtain the same structure ordering as at $T=0$ for neutral (charged) $C_{20}$; at $T\simeq1100$ (700) K the free-energy curves of the three isomers cross, yielding the ring as the most stable structure, followed by the bowl and the cage, in order of increasing energy. In the case of $C_{20}^-$, the bowl and the cage are almost degenerate. Within PBE, the ring is the most stable structure at all temperatures for both neutral and charged $C_{20}$, followed by the
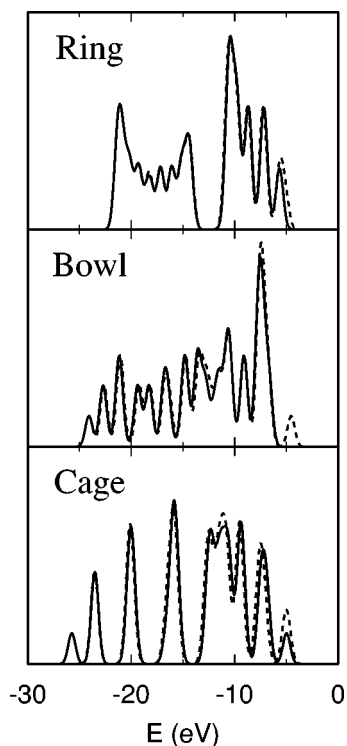


FIG. 2. Density of valence occupied states (arbitrary units) of the three $C_{20}$ isomers. Solid and dotted lines indicate results for the neutral and negatively charged clusters. The bottom of the valence bands of the neutral and charged clusters has been arbitrarily aligned for each isomer. We used a Gaussian broadening of width 0.5 eV.
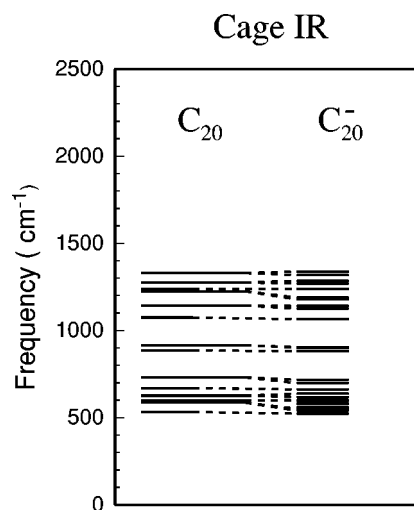


FIG. 3. Vibrational frequencies of the IR active modes of the cage isomer, computed using the local-density approximation. The left and right portion of the picture show the frequencies of the neutral and charged species, respectively. Dotted lines indicate the correspondence between the modes of $C_{20}$ and $C_{20}^-$. The modes are either singly or doubly degenerate. Doubly degenerate modes have been represented with a line twice as long as that indicating singly degenerate modes.
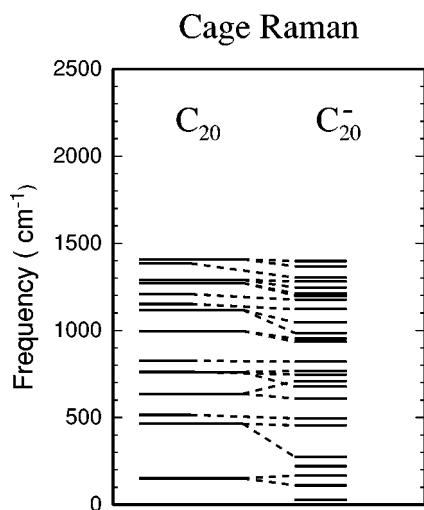
## Cage Raman



FIG. 4. Vibrational frequencies of the Raman modes of the cage isomer, computed using the local-density approximation. The left and right portion of the picture show the frequencies of the neutral and charged species, respectively. Dotted lines indicate the correspondence between the modes of $C_{20}$ and $C_{20}^-$. The mode degeneracy is represented as in Fig. 3.

## Ring IR



FIG. 6. Vibrational frequencies of the IR active modes of the ring isomer, computed using the local-density approximation. The left and right portion of the picture show the frequencies of the neutral and charged species, respectively. Dotted lines indicate the correspondence between the modes of $C_{20}$ and $C_{20}^-$. The mode degeneracy is represented as in Fig. 3.

bowl and the cage, the free-energy difference between the ring and the bowl being larger in the case of charged molecules. Our findings are consistent with recent measurements detecting $C_{20}$ clusters with a ring structure in graphite laser vaporization sources,[6–8] where the clusters are negatively charged and expected to be at high temperature.

In order to estimate free energies for neutral $C_{20}$ with different theoretical models, we used the value of $E_0$ obtained with different first-principles calculations (see Table I) and evaluated the zero-point motion and the entropic terms at the LDA level.[25] When doing so, we got different crossing points ($T_c$) for the three free-energy curves but in all cases the same structure ordering above $T_c$. As mentioned above,

in the case of some gradient-corrected results, the ring is already the most stable structure at zero temperature and we did not observe any crossing. This indicates that, irrespective of the theoretical approximation used to evaluate the cluster total energy at $T=0$, the ring structure is predicted to be the most abundant species in molecular beams at high temperature ($T \gtrsim T_c$). We note that similar conclusions were drawn by Brabec *et al.*[11] in a study of precursors to $C_{60}$ fullerene formation, using semiempirical methods. Using quantum chemistry methods Martin, El-Yazal, and J. P. François[16] found that up to $\simeq 1700$ K the bowl is favored with respect to the ring and the cage; above this temperature the ring becomes instead more stable, followed by the bowl and the cage.
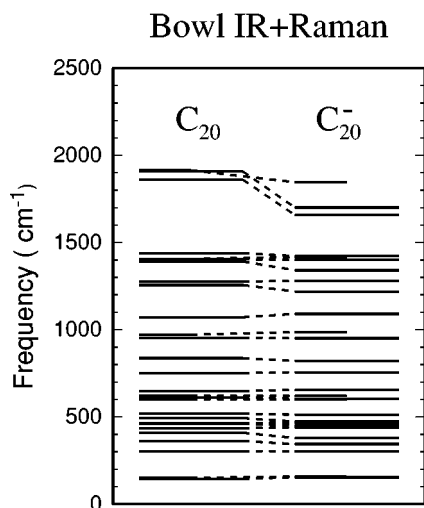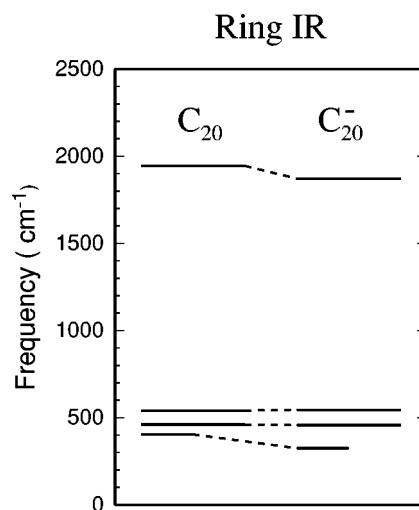
## Bowl IR+Raman



FIG. 5. Vibrational frequencies of infrared and Raman active modes of the bowl isomer, computed using the local-density approximation. The left and right portion of the picture show the frequencies of the neutral and charged species, respectively. Dotted lines indicate the correspondence between the modes of $C_{20}$ and $C_{20}^-$. The mode degeneracy is represented as in Fig. 3.
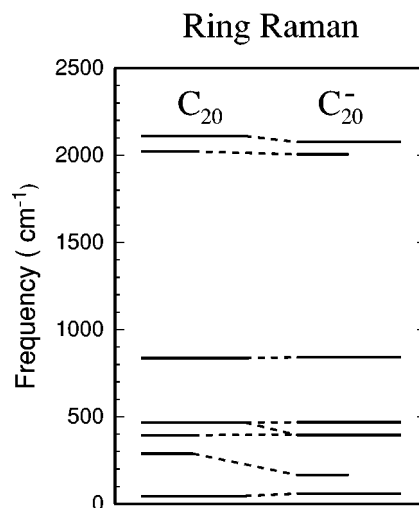
## Ring Raman



FIG. 7. Vibrational frequencies of the Raman modes of the ring isomer, computed using the local-density approximation. The left and right portion of the picture show the frequencies of the neutral and charged species, respectively. Dotted lines indicate the correspondence between the modes of $C_{20}$ and $C_{20}^-$. The mode degeneracy is represented as in Fig. 3.

TABLE V. Vibrational frequencies of the cage, bowl, and ring isomers of neutral $C_{20}$, computed using the local-density approximation. The modes are classified according to the irreducible representations of the symmetry group: $D_{3d}$, $C_{5v}$, and $D_{10h}$ for the cage, bowl, and ring, respectively.

| Isomer | Vibrational frequencies (cm$^{-1}$) |
|---|---|
| Cage | $151(e_g)$ $353(a_{2g})$ $464(e_g)$ $515(a_{1g})$ $532(a_{2u})$ $559(a_{1u})$ $586(e_u)$ $598(e_u)$ $601(a_{1u})$ $626(e_u)$ |
| | $636(e_g)$ $670(a_{2u})$ $712(a_{2g})$ $731(e_u)$ $761(e_g)$ $762(a_{1g})$ $826(a_{1g})$ $886(a_{2u})$ $916(e_u)$ $996(e_g)$ |
| | $1075(a_{2u})$ $1117(e_g)$ $1143(e_u)$ $1152(a_{1g})$ $1191(a_{1u})$ $1208(a_{1g})$ $1212(a_{2g})$ $1225(e_u)$ $1238(a_{2u})$ |
| | $1272(e_g)$ $1275(e_u)$ $1290(e_g)$ $1320(a_{1u})$ $1329(e_u)$ $1384(a_{1g})$ $1408(e_g)$ |
| Bowl | $145(e_2)$ $150(a_1)$ $303(e_2)$ $362(e_1)$ $409(e_2)$ $435(e_1)$ $459(e_1)$ $463(e_2)$ $469(a_2)$ $478(a_2)$ $493(e_2)$ |
| | $518(e_1)$ $602(a_1)$ $612(e_1)$ $620(a_1)$ $648(e_2)$ $752(e_2)$ $780(a_2)$ $837(e_1)$ $954(e_2)$ $972(a_1)$ $1071(e_1)$ |
| | $1256(e_2)$ $1277(e_2)$ $1391(e_1)$ $1404(e_2)$ $1406(a_1)$ $1439(e_1)$ $1463(a_2)$ $1860(e_2)$ $1907(e_1)$ $1914(a_1)$ |
| Ring | $45(e_{2g})$ $52(e_{2u})$ $124(e_{3u})$ $132(e_{3g})$ $221(e_{4g})$ $226(e_{4u})$ $288(a_g)$ $301(b_g)$ |
| | $303(b_u)$ $334(b_u)$ $343(b_g)$ $394(a_g)$ $397(e_{4g})$ $399(e_{4u})$ $404(a_u)$ $445(e_{3u})$ |
| | $446(e_{3g})$ $460(e_{1u})$ $465(e_{2g})$ $466(e_{1g})$ $470(e_{2u})$ $541(e_{1u})$ $836(e_{2g})$ $1145(e_{3u})$ |
| | $1416(e_{4g})$ $1555(b_u)$ $1925(b_u)$ $1944(e_{1u})$ $2007(e_{4g})$ $2022(a_g)$ $2104(e_{3u})$ $2110(e_{2g})$ |

In order to investigate possible changes in the ring geometry as the temperature increases, we have performed molecular-dynamics simulations and heated the ring structure up to about 1100 K. At this temperature we have monitored the system geometry for about 2 ps. We found that the molecule shows an appreciable dimerization also at high temperature, indicating that the geometry optimized at $T = 0$ is representative of the cluster geometry (acetylenic) also at higher temperatures.

### IV. $C_{2n}$ RINGS, $n = 9-12$

Recently the highest vibrational frequency of $C_{20}$ in molecular beams has been measured,[9] and found to lie slightly above 2000 cm$^{-1}$. The observed frequency led the authors of Ref. 9 to postulate the presence of $C_{20}$ clusters in a bicyclic geometrical arrangement. This assumption was motivated by the marked difference between the spectra of $C_{18}$ and $C_{20}$, which were attributed to differences in the topology of the two clusters. Since $C_{18}$ is believed to be a ring, it

was argued that $C_{20}$ should not have a ring structure and that a possible geometry leading to vibrational frequencies in the measured range (i.e., $\simeq 2000$ cm$^{-1}$) could be a bicyclic ring. It was also suggested that a transition from monocyclic to bicyclic carbon rings occurs when the number of atoms equals 20. However, it was pointed out that the spectra of $C_{22}$ and $C_{26}$ on one hand, and $C_{20}$ and $C_{24}$ on the other hand, reveal some differences in the structural properties of the two groups of clusters. In what follows we argue that these differences, together with those between $C_{20}$ and $C_{18}$, can be understood in terms of the electronic structure of $C_{2n}$ clusters in a monocyclic ring configuration, when $n = 9-12$ is either odd or even.

The valence occupied states of a linear chain of carbon atoms (oriented in the $x$ direction) are characterized by $\sigma$ and $\pi$ states, coming, respectively, from the hybridization of $s$ and $p_x$, and from $p_y$ and $p_z$ atomic orbitals. In a linear chain with bonds of equal length, $p_y$ and $p_z$ orbitals are degenerate and, therefore, most $\pi$ states are fourfold degenerate (ignor-

TABLE VI. Vibrational frequencies of the cage, bowl, and ring isomers of negatively charged $C_{20}$, computed using the local density approximation. The modes are classified according to the irreducible representations of the symmetry group: $C_{2h}$, $C_{5v}$, and $D_{10h}$ for the cage, bowl, and ring, respectively.

| Isomer | Vibrational frequencies (cm$^{-1}$) |
|---|---|
| Cage | $28(b_g)$ $111(a_g)$ $167(b_g)$ $221(b_g)$ $274(a_g)$ $455(b_g)$ $495(a_g)$ $523(b_u)$ $540(b_u)$ $551(a_u)$ |
| | $560(a_u)$ $580(a_u)$ $597(b_u)$ $601(a_u)$ $609(a_g)$ $618(b_u)$ $638(a_u)$ $662(b_u)$ $678(a_g)$ $698(a_u)$ |
| | $709(b_g)$ $717(b_u)$ $746(a_g)$ $767(b_g)$ $821(a_g)$ $881(b_u)$ $900(a_u)$ $904(b_u)$ $935(a_g)$ $953(b_g)$ |
| | $985(b_g)$ $1046(a_g)$ $1065(b_u)$ $1122(a_g)$ $1126(a_u)$ $1141(b_u)$ $1176(a_g)$ $1178(a_u)$ $1189(b_u)$ |
| | $1196(b_g)$ $1201(b_g)$ $1212(a_g)$ $1234(a_u)$ $1238(a_u)$ $1244(b_u)$ $1246(b_g)$ $1269(a_u)$ |
| | $1281(a_g)$ $1285(b_u)$ $1303(a_g)$ $1318(b_u)$ $1338(a_u)$ $1367(a_g)$ $1398(b_g)$ |
| Bowl | $153(e_2)$ $158(a_1)$ $302(e_2)$ $344(e_1)$ $379(e_2)$ $440(e_1)$ $452(e_1)$ $468(a_2)$ $464(e_1)$ $491(e_2)$ $473(a_2)$ |
| | $513(e_2)$ $599(a_1)$ $605(e_1)$ $621(a_1)$ $655(e_2)$ $755(e_2)$ $780(a_2)$ $822(e_1)$ $951(e_2)$ $986(a_1)$ $1091(e_1)$ |
| | $1219(e_2)$ $1280(e_2)$ $1341(e_1)$ $1394(a_2)$ $1400(e_2)$ $1416(a_1)$ $1422(e_1)$ $1658(e_2)$ $1701(e_1)$ $1846(a_1)$ |
| Ring | $59(e_{2g})$ $69(e_{2u})$ $133(e_{3u})$ $140(e_{3g})$ $166(a_g)$ $228(e_{4g})$ $232(e_{4u})$ $303(b_u)$ |
| | $307(b_g)$ $317(b_g)$ $325(a_u)$ $344(b_u)$ $372(e_{4u})$ $393(e_{1g})$ $398(a_g)$ $403(e_{3g})$ |
| | $405(e_{4g})$ $411(e_{2u})$ $449(e_{3u})$ $457(e_{1u})$ $469(e_{2g})$ $545(e_{1u})$ $841(e_{2g})$ $1153(e_{3u})$ |
| | $1434(e_{4g})$ $1592(b_u)$ $1865(b_u)$ $1872(e_{1u})$ $1967(e_{4g})$ $2005(a_g)$ $2071(e_{3u})$ $2076(e_{2g})$ |
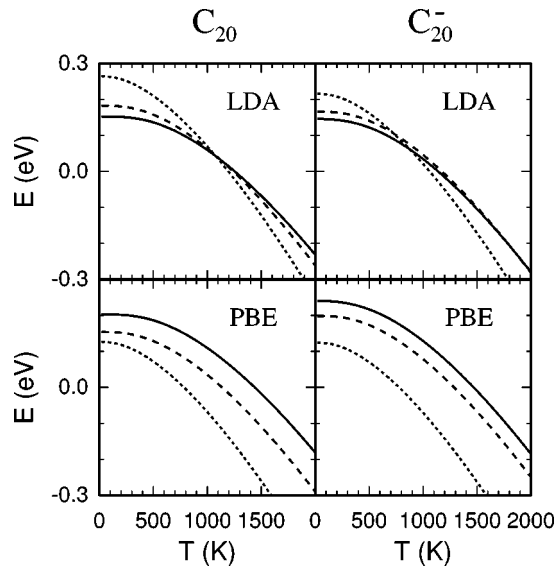
FIG. 8. Free energy of the neutral (left panel) and charged (right panel) $C_{20}$ isomers as a function of temperature ($T$), as calculated by using an harmonic approximation and two different functionals (LDA and PBE) for the exchange and correlation energy (see text). Solid, dotted and dashed lines indicate the cage, bowl, and ring isomers, respectively.

ing spin). If the chain has a finite curvature, i.e., is bent to form a ring, the $p_y$-$p_z$ degeneracy is lifted and each group of four $\pi$ states splits into two pairs of eigenvalues, separated by a gap, which we call a bending gap. In our calculations, for curvatures corresponding to $C_{18}$ and $C_{20}$, we found that the average bending gap is about 0.06 and 0.03 eV, respectively (see Table VII). This is much smaller than the energy gap separating groups of four $\pi$ eigenvalues, which is generally larger than 1 eV (see Table VII). In general, for $C_{2n}$ clusters, $n=9$–12, the highest occupied (HOMO) and lowest unoccupied (LUMO) molecular orbitals of the ring are separated by a small bending gap if $n$ is even, whereas for $n$ odd

they are separated by a much larger gap (e.g., $\simeq 2.2$ eV in the case of $C_{18}$) between groups of four eigenvalues. Therefore, the total energy of $C_{2n}$ with $n$ even can be lowered by dimerization, whereas that of $C_{2n}$ with $n$ odd, having a large HOMO-LUMO gap in a cumulenic configuration, is not expected to do so. This is precisely what we found in our LDA calculations: starting from cumulenic geometries for a $C_{20}$ and a $C_{18}$ ring, the optimized structures turned out to be different. $C_{20}$ showed an appreciable dimerization, whereas $C_{18}$ did not, having all bonds of equal length (1.28 Å). Furthermore, a geometry optimization of $C_{18}$ starting from a dimerized structure led as well to a nondimerized ground state. Consistently with the prediction of special stability for $C_{4n+2}$ rings,[8] we found that the total energy of $C_{18}$ is lower than that of $C_{20}$ by 0.04 eV/atom. In summary, we expect $C_{2n}$ rings with odd $n$ to be cumulenic rings and those with even $n$ to be acetylenic rings, for $n=9$–12. This will affect the vibrational spectra of these clusters, and in particular their high-frequency region, cumulenic rings having a lower maximum frequency than acetylenic rings. These results can account for the qualitative differences found in measured photoelectron spectra[9] of $C_{2n}$ clusters, with $n=9$–12, without invoking bicyclic geometries. Furthermore the measured[9] maximum frequency of $C_{20}$ agrees well with our results for the monocyclic ring (see Table V).

Finally, we computed the total energies of $C_{20}$ in the two bicyclic ring structures sharing one bond and found them to be much higher (about 2.5–3.5 eV) than that of the monocyclic ring, consistently with QMC results.[26] Tight-binding optimizations found instead monocyclic and bicyclic ring geometries that are almost degenerate in energy.[18]

## V. CONCLUSIONS

We have presented first-principles calculations of electronic and vibrational spectra of neutral and negatively charged $C_{20}$ isomers, and free-energy calculations using different theoretical models. Both series of spectra exhibit dis-

TABLE VII. Single-particle energies (eV) of $\sigma$ ($[\epsilon_i^\sigma]_o$) and $\pi$ ($[\epsilon_i^\pi]_o$) valence occupied states and of some $\pi$ empty states ($[\epsilon_i^\pi]_e$) for $C_{20}$ and $C_{18}$ neutral monocyclic rings. Eigenvalue degeneracies are given between parentheses.

| | $C_{20}$ |
|---|---|
| $[\epsilon_i^\sigma]_o$ | -21.37  -21.23 ($\times 2$)  -20.81 ($\times 2$)  -20.14 ($\times 2$)  -19.28 ($\times 2$)  -18.45 |
| | -18.06  -17.15 ($\times 2$)  -16.09 ($\times 2$)  -15.15 ($\times 2$)  -14.49 ($\times 2$)  -14.25 |
| $[\epsilon_i^\pi]_o$ | -10.66  -10.64  -10.43 ($\times 2$)  -10.42 ($\times 2$)  -9.76 ($\times 2$)  -9.75 ($\times 2$) |
| | -8.68 ($\times 2$)  -8.64 ($\times 2$)  -7.20 ($\times 2$)  -7.14 ($\times 2$)  -5.68  -5.63 |
| $[\epsilon_i^\pi]_e$ | -4.90  -4.85  -3.12 ($\times 2$)  -3.04 ($\times 2$) |
| | $C_{18}$ |
| $[\epsilon_i^\sigma]_o$ | -21.47  -21.28 ($\times 2$)  -20.75 ($\times 2$)  -19.92 ($\times 2$)  -18.86 ($\times 2$)  -17.67 ($\times 2$) |
| | -16.46 ($\times 2$)  -15.37 ($\times 2$)  -14.56 ($\times 2$)  -14.27 |
| $[\epsilon_i^\pi]_o$ | -10.72  -10.70  -10.45 ($\times 2$)  -10.40 ($\times 2$)  -9.60 ($\times 2$)  -9.56 ($\times 2$)  -8.24 ($\times 2$) |
| | -8.18 ($\times 2$)  -6.39 ($\times 2$)  -6.30 ($\times 2$) |
| $[\epsilon_i^\pi]_e$ | -4.10 ($\times 2$)  -4.09 ($\times 2$) |

tinctive features that could be used as fingerprints for the presence of a given geometrical structure in, e.g., molecular beams or thin films. Furthermore, free-energy calculations indicate that the ring structure is the most abundant species for both neutral and negatively charged clusters at high temperature. Molecular-dynamics simulations have shown that the dimerized geometry of the neutral ring persists at high temperatures. Our results are consistent with several recent experiments revealing the presence of ring structures in graphite laser vaporization sources, and reconcile theoretical and experimental viewpoints on the relative stability of the three $C_{20}$ isomers.

This work also confirms the high sensitivity of the energy ordering of $C_{20}$ isomers on the treatment of correlation used in the calculations, even when geometries are consistently optimized.

Finally, we rationalized recent photoelectron data arguing that $C_{2n}$ clusters with $n = 9-12$ show either an alternation of short and long bonds if $n$ is even, or all bonds of equal length, if $n$ is odd.

*Present address: Colorado State University, Atmospheric Science Department, Fort Collins, CO 80523.

[1] R. F. Curl, Philos. Trans. R. Soc. London **343**, 19 (1993).

[2] G. von Helden, N.G. Gotts, and M.T. Bowers, Nature (London) **363**, 60 (1993).

[3] V. Paillard, P. Melinon, V. Dupuis, J.P. Perez, A. Perez, and B. Champagnon, Phys. Rev. Lett. **71**, 4170 (1993).

[4] See, e.g., Mat. Sci. Forum **232**, special issue on XXX, edited by K. Sattler (1996).

[5] G. Benedek, L. Colombo, and S. Serra, J. Chem. Phys. **106**, 2311 (1997).

[6] G. von Helden, M.T. Hsu, N.G. Gotts, P.R. Kemper, and M.T. Bowers, Chem. Phys. Lett. **204**, 15 (1993).

[7] J.N. Hunter, J.L. Fey, and M.F. Jarrold, J. Phys. Chem. **97**, 3460 (1993); Science **260**, 784 (1993).

[8] S. Yang, K.J. Taylor, M.J. Craycraft, J. Conceicao, C.L. Pettiette, O. Cheshnovsky, and R.E. Smaley, Chem. Phys. Lett. **144**, 431 (1988).

[9] H. Handschuh, G. Ganteför, B. Kessler, P.S. Bechthold, and W. Eberhardt, Phys. Rev. Lett. **74**, 1095 (1995).

[10] C.J. Brabec, E.B. Anderson, B.N. Davidson, S.A. Kajihara, Q.-M. Zhang, J. Bernholc, and D. Tomanek, Phys. Rev. B **46**, 7326 (1992).

[11] P.R. Taylor, E. Bylaska, J.H. Weare, and R. Kawai, Chem. Phys. Lett. **235**, 558 (1995).

[12] Z. Wang, P. Day, and R. Pachter, Chem. Phys. Lett. **248**, 121 (1996).

[13] K. Raghavachari, D.L. Strout, G.K. Odom, G.E. Scuseria, J.A. Pople, B.G. Johnson, and P.M.W. Gill, Chem. Phys. Lett. **214**, 357 (1993).

[14] J.C. Grossman, L. Mitas, and K. Raghavachari, Phys. Rev. Lett. **75**, 3870 (1995); L. Mitas and J.C. Grossman, *Recent Advances in Computational Chemistry* (in press).

[15] V. Parasuk and J. Almlöf, Chem. Phys. Lett. **184**, 187 (1991).

[16] J.M.L. Martin, J. El-Yazal, and J-P. François, Chem. Phys. Lett. **248**, 345 (1996).

[17] R.O. Jones and G. Seifert, Phys. Rev. Lett. **79**, 443 (1997).

[18] M. Sawtarie, M. Menon, and K.R. Subbaswamy, Phys. Rev. B **49**, 7739 (1994).

[19] J. Perdew, K. Burke, and M. Ernzerhof, Phys. Rev. Lett. **77**, 3865 (1996).

[20] D.C. Patton, D.V. Porezag, and M.R. Pederson, Phys. Rev. B **55**, 7454 (1997).

[21] D.R. Hamann, Phys. Rev. B **55**, R10 157 (1997).

[22] G. Makov and M.C. Payne, Phys. Rev. B **51**, 4014 (1995).

[23] We used the first-principles molecular-dynamics program JEEP (http://irrmawww.epfl.ch/fg/jeep/jeep.html), with a norm-conserving pseudopotential [D. Hamann, Phys. Rev. B **40**, 2980 (1989); cutoff radii of 0.85 and 0.80 a.u. for $s$ and $p$ orbitals, respectively].

[24] See, e.g., *Statistical Mechanics*, K. Huang, 2nd ed. (Wiley, New York, 1987), p. 184.

[25] We checked the sensitivity of free-energy calculations to fine details of the computed spectra by repeating our computations using harmonic frequencies obtained at the HF level (Ref. 11). The results discussed in the text were unchanged.

[26] J.C. Grossman and L. Mitas (private communication).